Growth and Saturation of Convective Modes of the Two-Plasmon Decay Instability in Inertial Confinement Fusion

R. Yan,[1] A. V. Maximov,[1] C. Ren,[1,2] and F. S. Tsung[3]

[1]*Department of Mechanical Engineering and Laboratory for Laser Energetics, University of Rochester, Rochester, New York 14627, USA*

[2]*Department of Physics and Astronomy, University of Rochester, Rochester, New York 14627, USA*

[3]*Department of Physics and Astronomy, University of California, Los Angeles, California 90095, USA*

(Received 13 April 2009; published 20 October 2009)

Particle-in-cell (PIC) and fluid simulations of two-plasmon decay (TPD) instability under conditions relevant to inertial confinement fusion show the importance of convective modes. Growing at the lower density region, the convective modes can cause pump depletion and are energetically dominant in the nonlinear stage. The PIC simulations show that TPD saturates due to ion density fluctuations, which can turn off TPD by raising the instability threshold through mode coupling.

DOI: 10.1103/PhysRevLett.103.175002 PACS numbers: 52.57.−z, 52.38.Dx, 52.65.Rr

Effective compression of inertial confinement fusion (ICF) targets requires fuel shells in low adiabatic states during implosion. Energetic (hot) electrons generated from laser-plasma interactions can preheat the shell and degrade the implosion. For direct-drive ICF the two-plasmon decay (TPD) instability is a significant concern as a hot electron source due to its low threshold [1] and high electron energy [2,3]. TPD remains a concern for the indirect-drive experiments currently underway at the National Ignition Facility (NIF) [4] aiming to achieve ignition and fusion energy gain for the first time. It is also a potential roadblock to shock ignition, a high-gain scheme that can lead to a more economic fusion reactor [5,6]. Linear theory on TPD in an inhomogeneous plasma has been developed to predict the instability threshold, growth rates and unstable mode number range [1,7,8]. These work focused on absolute modes, which can grow without limit in the linear stage and were thought to be more important than convective modes [9,10], which can grow only to a finite amplitude before convecting out of the growth region. Nonlinear phenomena including saturation and hot electron generation in TPD were first studied with particle-in-cell (PIC) simulations in the regime of high laser intensity (I) and short density scale length (L) [11]. The saturation mechanisms found were ion density fluctuations, causing the plasmons coupled to shorter wavelength modes that are Landau damped, and density profile steepening. Fluid simulations based on the Zakharov equations [12,13] were also used to study the long-time evolution of TPD, especially the nonlinear saturation due to secondary instabilities of plasmons.

However, current generation direct-drive experiments found a wide TPD spectrum, with modes of perpendicular mode number $k_\perp$ larger than the cutoff for the absolute modes, and it was attributed to the nonlinear evolution of TPD [14]. In this Letter, we present PIC simulations with I and L relevant to these experiments that show a similar wide spectrum, in both linear and nonlinear stages, for the first time. Using a new fluid code that solves the full set of linear equations for TPD, we clearly show that these large $k_\perp$ modes are convective. The PIC simulations show that even before reaching the amplitude limit set by convection, the convective modes become energetically dominant and can reduce absolute mode growth via pump depletion. These results show that the convective modes of TPD are important to the performance of current and future direct-drive experiments. They also caution against automatically disregarding convective modes to focus on absolute modes when studying an instability.

We have performed a series of TPD simulations for different parameters with the full PIC code OSIRIS [15]. Here we focus on two simulations. The large-L case has parameters representative of the direct-drive experiments at the OMEGA laser facility with $I = 10^{15}$ W/cm^2 and a linear density profile with the density scale length at the quarter-critical surface $L \equiv n_0/(\partial n_0/\partial x)|_{n_0=n_c/4} = 150$ μm. Since time and length in the simulations scale with $1/\omega_0$ and c/ω_0 where ω_0 is the laser frequency, these I and L are for a laser wavelength of $\lambda = 1/3$ μm. The electron and ion temperatures are $T_e = T_i = 2$ keV. Ion mass $M_i/(Zm_e) = 3410$ can represent fully ionized CH (Z is the ion ionization state and m_e the electron mass.) The simulation box is 38.2 μm long and 63.7 μm wide. The linear density profile goes from $0.210n_c$ to $0.273n_c$ with a 0.53 μm vacuum region in front of the $n_0 = 0.210n_c$ surface. The grid is 3600×6000 and 80 particles per cell are used for each species. The small-L case has $I = 2 \times 10^{15}$ W/cm^2, $L = 25$ μm, $T_e = T_i = 1$ keV, and $M_i/(Zm_e) = 1836$. The density range is essentially the same with a box size of 8.5 μm $\times$ 8.5 μm and a grid of 1600×1600. For both large and small-L cases, the laser comes from the left boundary ($x = 0$) as a plane wave and polarized in the y direction. The rise times are $100/\omega_0$ (large L) and $6.28/\omega_0$ (small L). Periodic boundary con-

ditions (BC) are used for the y direction. In the x direction open BC's are used for fields and thermal reflecting BC's for particles.

For these two cases, two different theories based on the same linear TPD equations [7,8] give similar growth rates and unstable region for the absolute modes [Figs. 1(a) and 1(b)]. For the large-L case, the unstable modes have $k_\perp < 0.2$–$0.3\omega_0/c$ and the dominant mode is at $k_\perp \approx 0.1\omega_0/c$. However, our PIC simulation shows a broader spectrum with the cutoff moved to $1.4\omega_0/c$ [Fig. 1(a)]. All modes observed in the PIC simulations fall on the universal hyperbola for TPD [16] but the larger-$k_\perp$ modes are in the lower-n_0 region [Fig. 1(c)]. The relation between $k_\perp$ and n_0 can be well described by the TPD dispersion relation for the fastest-growing mode in a homogeneous plasma [16]. In the small-$k_\perp$ region the PIC simulation shows a smaller growth rate than that predicted by the theories. This is due to pump depletion caused by the larger-$k_\perp$ modes in the lower-n_0 region. The growth rates from the simulation would agree with the theories if the observed laser amplitude near the $n_0 = 0.25n_c$ surface were used. For the small-L case, there is less growth in the large-$k_\perp$ modes, less pump depletion and better agreement in the growth rates of the small-$k_\perp$ modes.

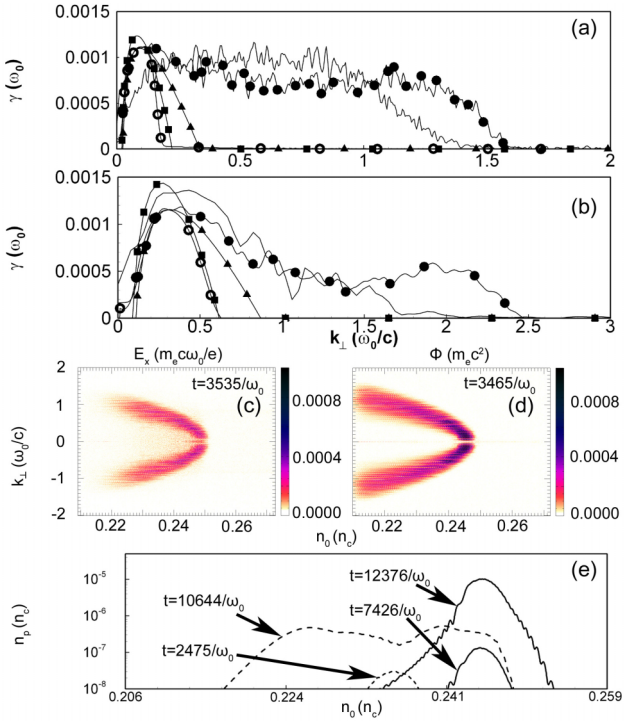

FIG. 1 (color online). (a) and (b) Comparison of TPD growth rates for the large-L (a) and the small-L (b) cases. Solid line: PIC simulation; solid circle: fluid simulation seeded with uniform random initial perturbation; open circle: fluid simulation seeded with δ-function initial perturbation; solid triangle: linear theory (Ref. [7]); square: linear theory (Ref. [8]). (c) and (d) Spectrum in the $n_0(x) - k_y$ space for E_x in the PIC simulation (c) and ϕ in the fluid simulation (d) of the large-L case. (e) The evolution of two different modes, $k_\perp = 0.18\omega_0/c$ (solid line) and $k_\perp = 0.75\omega_0/c$ (dashed line) in a fluid simulation for the large-L case.

To determine the nature of the large-$k_\perp$ modes observed in the PIC simulations, we have developed a fluid code to numerically solve the full linear PDE system that was used as the starting point in [1,7]. In dimensionless form the equations are

$$\frac{\partial \psi}{\partial t} = \phi - 3v_e^2 \frac{n_p}{n_0} - \mathbf{v_0} \cdot \nabla \psi, \tag{1}$$

$$\frac{\partial n_p}{\partial t} = -\nabla \cdot (n_0 \nabla \psi) - \mathbf{v_0} \cdot \nabla n_p, \tag{2}$$

$$\nabla^2 \phi = n_p, \tag{3}$$

where n_p is the density perturbation, ϕ the electrostatic potential, ψ the velocity potential, v_e the electron thermal velocity, v_0 the electron oscillation velocity in the laser field. These equations are first Fourier-transformed in y and each $k_\perp$ mode is then solved in the (x, t) space. We assume that all electrostatic waves have already been strongly damped or absorbed before they could reach either longitudinal boundary; thus we let $\partial_x \psi = 0$, $\partial_x \phi = 0$, $n_p = 0$ for both longitudinal boundaries. The fluid simulations contain similar range of n_0 as in the PIC simulations and start with initial density perturbations of various x profiles $n_{\rm pi}(x)$. Landau damping is not included in this code.

When $n_{\rm pi}$ has a uniformly random amplitudes in x, the growth rates from the fluid simulations agree with the theories in the small-$k_\perp$ region but are still substantial in the large-$k_\perp$ region, similar to the PIC simulations [Figs. 1(a) and 1(b)]. As in the PIC simulations, the larger-$k_\perp$ modes grow at the lower density region [Fig. 1(d)]. The cutoffs at large $k_\perp$ in the fluid spectra are determined by the lower limit of n_0 in the simulations while those in the PIC spectra are determined by Landau damping. This leads to lower growth rates for modes near the cutoff in the PIC simulations. When $n_{\rm pi}$ is a δ-function in the $n_c/4$-surface, the fluid simulations agree with the theories well, showing growth only in the low-$k_\perp$ region.

The fluid simulations further show that the large-$k_\perp$ modes are convective with a different linear growth pattern from the small-$k_\perp$ absolute modes. Figure 1(e) shows the evolution of two modes of $k_\perp = 0.18\omega_0/c$ and $0.75\omega_0/c$ in the large-L case, with $n_{\rm pi}$ for both modes placed locally at $n_0 = 0.233n_c$, which is the homogeneous resonant density for $k_\perp = 0.75\omega_0/c$. The $k_\perp = 0.18\omega_0/c$ mode moves to its resonant region (just below $1/4n_c$) and then grows exponentially with the same envelope shape and without limit, as expected from an absolute mode. The $k_\perp = 0.75\omega_0/c$ mode first grows at its resonant region exponentially as if the inhomogeneity is not present. When the amplification reaches $\sim$100 it saturates with the peak flattening first and then splitting into two peaks that move away from the resonant region. This type of behaviors is typical of convective modes of parametric instabilities in an inhomogeneous medium. Indeed, Eqs. (1)–(3)

can be cast into the standard three-wave model that was used to study the convective modes [9]. Assuming that each variable Q (i.e., ψ, ϕ, or n_p) can be written as envelopes of two well-defined daughter waves, $Q(x,y,t) = (1/2)\{Q_1(x,t)\exp[i(\omega_1 t - \int_0^x k_{x1}(x')dx' - k_\perp y)] + Q_2(x,t)\times \exp[i(\omega_2 t - \int_0^x k_{x2}(x')dx' + k_\perp y)]\} + \text{c.c.}$, and only keeping the first-order terms involving $\partial_t Q$, $\partial_x Q$, v_0, and $\partial_x n_0$, we can obtain from Eqs. (1)–(3) the standard form of the three-wave model in terms of $a_{1,2} \equiv \phi^*_{1,2}\sqrt{k_y|v_0||\omega_{1,2}/\omega_{2,1} - k^2_{1,2}/k^2_{2,1}|/4}$,

$$\left[\frac{\partial}{\partial t} + v_{1,2}(x)\frac{\partial}{\partial x} + \gamma_{1,2}(x)\right]a_{1,2}(x,t) = \gamma(x)a^*_{2,1}(x,t)\exp\left(\int_0^x i\kappa(x')dx'\right), \quad (4)$$

where $v_{1,2}$ are the longitudinal group velocities of the two daughter plasma waves and the mismatch $\kappa(x) \equiv k_0(x) - k_{x1}(x) - k_{x2}(x)$ [$k_0(x)$ is the laser wave number at x]. Here we have combined terms due to density inhomogeneity and damping into $\gamma_{1,2}$, with $\gamma_{1,2} = \nu - \partial_x n_0 \omega_{1,2} k_{x1,2}/(2n_0 k^2_{1,2}) - \partial_x n_0/(4k_{x1,2}\omega_{1,2})$ and ν is the combined damping rate of collisional and Landau damping. The coupling constant γ is found to be

$$|\gamma|^2 = -\frac{1}{16}k^2_\perp v^2_0\left(\frac{\omega_2}{\omega_1} - \frac{k^2_2}{k^2_1}\right)\left(\frac{\omega_1}{\omega_2} - \frac{k^2_1}{k^2_2}\right), \quad (5)$$

where $k^2_{1,2} = k^2_\perp + k^2_{x1,2}$. For a linear mismatch, Eq. (4) can be analyzed to show [9,10] that the amplitude amplification for the convective modes before they split, the so-called Rosenbluth gain, is $g_R \sim \exp(\pi\Lambda)$, where $\Lambda = |\gamma|^2/(\kappa' v_1 v_2)$. For the convective TPD instability, κ' can be calculated from the dispersion relations of the two daughter waves, $\kappa' \equiv d\kappa/dx = (-1/(2k_0c^2) + 1/(6k_{x1}v^2_e) + 1/(6k_{x2}v^2_e))dn/dx$.

For a certain n_0, more than one pair of plasmons can develop in PIC or fluid simulations, as long as they can satisfy the matching conditions. However, the simulations also show that the dominant mode is well described by the TPD dispersion relation for the fastest-growing mode in a homogeneous plasma. Therefore we use the values of k_{x1} and k_{x2} from the homogeneous hyperbola to evaluate g_R for a certain $k_\perp$ mode. The leading term of Λ is thus found to be

$$\pi\Lambda \approx 2.15(1 - 0.008\,81T_{\text{keV}} - 0.0470T_{\text{keV}}\tilde{k}^2_\perp)\eta. \quad (6)$$

Here, $\eta \equiv (I_{14}\lambda_{\mu m}L_{\mu m}/T_{\text{keV}})/81.86$ is how much the parameters are above the absolute threshold [7], T_{keV} is T_e normalized to keV, and $\tilde{k}_\perp$ is $k_\perp$ normalized to ω_0/c. Our large-L case has $\eta \approx 3$ while the small-L case has $\eta \approx 2$. That $\Lambda \propto \eta$ was also found in Ref. [8]. But Eq. (6) shows that the dependence of Λ on $k_\perp$ is weak, which explains the relatively flat growth rate profile for the convective modes in Figs. 1(a) and 1(b). For the $k_\perp = 0.75\omega_0/c$ mode in Fig. 1(e), $g_R \approx 430$ gives the correct order of magnitude of the amplification in the fluid simulation. The difference is due to the approximation used in deriving Eq. (4) and the sensitive dependence of g_R on $k_{x1,2}$.

In the PIC simulations, however, nonlinear effects end the linear growth of the convective modes well before the convective limit is reached. For the $k_\perp = 0.75\omega_0/c$ mode in the large-L case, the gain is about $\sim$28 when it saturates. (The gain is calculated using the measured initial noise level, which is about the same as that in a 2 keV-plasma.) For these simulations, only small modification of the average density profile is observed. The main saturation mechanism for both absolute and convective modes in the PIC simulations is the ion density fluctuations [11]. When the large-L case is repeated with immobile ions, the convective modes can grow to the convective limit and their subsequent peak-splitting has been observed. Figure 2(a) plots together the evolution of E^2_x, integrated in the entire simulation box, and the ion density fluctuation $\delta n/n_0$ at $n_0 = 0.245n_c$ for the small-L case, showing a clear correlation between the two and a recurrence of TPD. Our large-L case is stopped after the first saturation of the electric field energy but its correlation with the δn growth is also observed. The recurrence of TPD was first observed by Langdon *et al.* [11].

Quantitatively, the driving of δn is found to follow the ion-acoustic equation, with the ponderomotive pressure of the plasma waves as the driver, $(\partial^2_t - C^2_s\nabla^2)\delta n = \nabla^2|\mathbf{E}_{\text{env}}|^2/16\pi M_i$, where $C^2_s = (ZT_e + 3T_i)/M_i$ is the sound speed, and $\mathbf{E}_{\text{env}}$ is the electric field envelope, time-averaged over the plasma frequency $\omega_0/2$. For the small-L

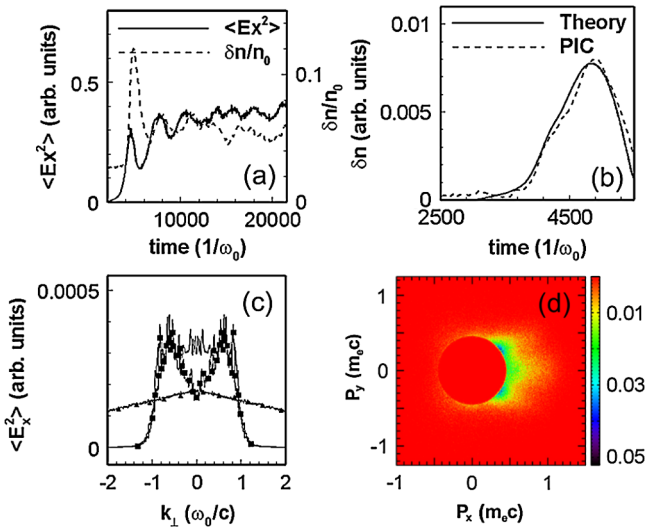

FIG. 2 (color online). (a) Correlation of $\langle E^2_x\rangle$ and δn at $n_0 = 0.245n_c$ in the small-L PIC simulation. (b) Comparison of $\delta n(k_\perp = 1.2\omega_0/c)$ at $n_0 = 0.247n_c$ predicted by the ion-acoustic equation and measured from the PIC for the small-L case. (c) Time evolution of the $k_\perp$ spectrum of $\langle E^2_x\rangle$ at 3 different times, $t = 141.4/\omega_0$ (triangle, amplified by a factor of 100), $t = 5656/\omega_0$ (square), and $t = 6363/\omega_0$ (solid line). (d) $p_x - p_y$ phase space distribution of electrons over 50 kev at $t = 5656/\omega_0$.

case, we have taken a time series of $\mathbf{E}$ from the PIC simulation to obtain $\mathbf{E}_{\rm env}$ at regular time intervals. We approximate ∇^2 in the ion-acoustic equation by $\partial^2/\partial y^2$ since the spatial variation in the y direction is much larger than in the x direction. We then solve the equation for individual $k_\perp$ modes. For the largest δn observed in the PIC simulation, located at $n_0 = 0.247 n_c$, the strongest modes agree well with δn predicted by the ion-acoustic model. Figure 2(b) shows the comparison of the time evolution of δn for the strongest mode at $k_\perp = 1.2\omega_0/c$, which is driven by the plasmons at $k_\perp = 0.6\omega_0/c$.

As δn grows, TPD saturates. There are several saturation mechanisms linked to δn. The ion density perturbations can act as stationary scattering centers upon which the plasmons scatter and up-shift in $\mathbf{k}$ to ranges where Landau damping is effective [11]. The density perturbations can also interact as (ion acoustic) waves with the plasmons to excite Langmuir wave turbulence [12]. Both mechanisms introduce effective energy sinks to the plasmon growth. However, energy sinks alone can only stop the growth and would leave the level of E_x constant. The decaying phases of E_x^2 in Fig. 2(a) indicate that significant δn should also turn off the plasmon growth. How exactly δn turns off TPD has been an open question. Here, we have found that δn raises the TPD threshold by breaking the transverse symmetry of n_0 and coupling modes of different $k_\perp$ that are previously independent. For a particular $\delta n = [\bar{n}_s \exp(ik_s y) + \text{c.c.}]/2$, the coupling is strongest between the two pairs of the plasmons of $k_\perp = k_s/2$, which are also the same modes that drive such a δn. The linear dispersion relation of this 4-plasmon system in the x-homogeneous limit shows that there is a threshold $\bar{n}_s$ above which the growth rate is zero. To compare this model with the PIC simulations, we have measured $\delta n(k_s)$ when E_x at $k_\perp = k_s/2$ starts to decrease. The measurement is made at a certain x and includes modes within $k_s \pm 5\% k_s$ to account for the neighboring modes' contribution to the coupling. For the small-L case, the modes are well localized in x by the density gradient. The largest δn is just below the $n_c/4$-surface and has a distinct peak at $k_s \approx 1.2\omega_0/c$ at saturation. The value of $|\bar{n}_s^{\rm sat}| \approx 0.013 n_c$ measured from the PIC simulation agrees with $|\bar{n}_s^{\rm sat}| = 0.0095 n_c$ predicted by the 4-plasmon model. For the large-L case, the $k_\perp$ spectra for δn and $\mathbf{E}$ at a certain x are wider. But the largest δn, right below the $n_c/4$ surface, also shows mainly a y variation. For the $k_\perp = 0.35\omega_0/c$ mode there the measured $|\bar{n}_s^{\rm sat}| \approx 0.003 n_{\rm cr}$ (at $t = 5600/\omega_0$) is also close to the prediction of $|\bar{n}_s^{\rm sat}| = 0.005 n_{\rm cr}$. Therefore, the density fluctuations turn off TPD as well as induce energy sinks. As TPD is turned off, δn decays, eventually making it possible for TPD to recur.

The convective modes are important energetically at the nonlinear stage. Figure 2(c) shows that for the large-L case, 75% of the electric field energy is in the convective modes ($k_\perp \geq 0.32\omega_0/c$) and the spectrum peaks at $k_\perp \sim 0.6\omega_0/c$ at $t = 5656/\omega_0$ (or $\sim$1 ps). The lack of small-$k_\perp$ modes is due to pump depletion. At this time, the total electric fields are still mainly of the plasmons from TPD and directional hot electrons can be observed in their phase space plot [Fig. 2(d)]. The particle data for electrons above 50 keV show that the hot electrons approximately follow a Maxwellian distribution $f(\epsilon) \sim \sqrt{\epsilon}\exp(-\epsilon/T_e)$ with $T_e =$ 36 keV. Including the particle energy lost to the thermal boundary, the fraction of laser energy transferred to the $\geq$50 keV electrons is $\sim$1% at this point. This plane wave absorption rate of the first ps is most likely an upper limit for TPD hot electron production since later on TPD would decay and becomes intermittent. The experiment measured value over $\sim$1 ns is less than 0.1% [2]. An accurate prediction of the absorption on the ns scale requires proper simulations of the long-term behaviors of the TPD recurrence and Langmuir turbulence evolution. At $t = 6363/\omega_0$, the scattering and secondary decaying of the plasmons cause the electric field spectrum to be flat below the Landau cutoff [Fig. 2(c)]. At this time the hot electrons are observed to be less directional. The long-term behavior of TPD remains a topic for future research.

We acknowledge useful conversations with R. Betti, W. Seka, A. Simon, and W. Mori. This work was supported by U. S. Department of Energy Grants No. DE-FG02-06ER54879, No. DE-FC02-04ER54789, No. DE-FG52-06NA26195, No. DE-FG52-09NA29552, and Cooperate Agreement No. DE-FC52-08NA28302. The research used resources of the National Energy Research Scientific Computing Center.

[1] C. S. Liu and Marshall N. Rosenbluth, Phys. Fluids **19**, 967 (1976)
[2] B. Yaakobi *et al.*, Phys. Plasmas **12**, 062703 (2005).
[3] C. Stoeckl *et al.*, Phys. Rev. Lett. **90**, 235002 (2003).
[4] E. I. Moses *et al.*, Eur. Phys. J. D **44**, 215 (2007).
[5] R. Betti *et al.*, Phys. Rev. Lett. **98**, 155001 (2007).
[6] L. J. Perkins *et al.*, Phys. Rev. Lett. **103**, 045004 (2009).
[7] A. Simon *et al.*, Phys. Fluids **26**, 3107 (1983).
[8] B. B. Afeyan and E. A. Williams, Phys. Plasmas **4**, 3827 (1997).
[9] M. N. Rosenbluth, Phys. Rev. Lett. **29**, 565 (1972).
[10] M. N. Rosenbluth, R. B. White, and C. S. Liu, Phys. Rev. Lett. **31**, 1190 (1973).
[11] A. B. Langdon, B. F. Lasinski, and W. L. Kruer, Phys. Rev. Lett. **43**, 133 (1979).
[12] D. F. DuBois, D. A. Russell, and H. A. Rose, Phys. Rev. Lett. **74**, 3983 (1995).
[13] D. A. Russell and D. F. DuBois, Phys. Rev. Lett. **86**, 428 (2001).
[14] W. Seka *et al.*, Phys. Plasmas **16**, 052701 (2009)
[15] R. A. Fonseca *et al.*, Lect. Notes Comput. Sci. **2331**, 342 (2002).
[16] William L. Kruer, *The Physics of Laser Plasma Interactions* (Westview Press, Boulder, CO, 2003)